



## OPEN ACCESS

EDITED BY  
Edit Dósa,  
Semmelweis University, Hungary

REVIEWED BY  
Xiaotong Hong,  
Southern Medical University, China  
Kakuya Kitagawa,  
Mie University, Japan

\*CORRESPONDENCE  
Joao A. C. Lima  
✉ jlima@jhmi.edu

RECEIVED 03 December 2025  
REVISED 10 February 2026  
ACCEPTED 23 February 2026  
PUBLISHED 17 March 2026

CITATION  
Kato Y, Chehab O, Ambale-Venkatesh B  
and Lima JAC (2026) Quantitative  
myocardial perfusion imaging across  
PET, SPECT, CMR, and CT.  
Front. Radiol. 6:1760241.  
doi: 10.3389/fradi.2026.1760241

COPYRIGHT  
© 2026 Kato, Chehab, Ambale-  
Venkatesh and Lima. This is an open-  
access article distributed under the  
terms of the [Creative Commons  
Attribution License \(CC BY\)](#). The use,  
distribution or reproduction in other  
forums is permitted, provided the  
original author(s) and the copyright  
owner(s) are credited and that the  
original publication in this journal is  
cited, in accordance with accepted  
academic practice. No use, distribution  
or reproduction is permitted which does  
not comply with these terms.

# Quantitative myocardial perfusion imaging across PET, SPECT, CMR, and CT

Yoko Kato<sup>1</sup>, Omar Chehab<sup>1</sup>, Bharath Ambale-Venkatesh<sup>2</sup> and Joao A. C. Lima<sup>1\*</sup>

<sup>1</sup>Division of Cardiology, Johns Hopkins University, Baltimore, MD, United States, <sup>2</sup>Department of Radiology, Johns Hopkins University, Baltimore, MD, United States

Recent clinical trials demonstrating the prognostic value of coronary computed tomography angiography (CCTA), and the limited incremental prognostic benefit of ischemia-guided revascularization over optimal medical therapy, have shifted focus away from functional testing. Nevertheless, myocardial perfusion assessment remains essential in patients with known or suspected coronary artery disease (CAD), microvascular dysfunction, ischemia with normal coronary arteries (INOCA), coronary anomalies, and cardiomyopathies. Advances in positron emission tomography (PET), cardiovascular magnetic resonance (CMR), and computed tomography (CT) now enable absolute quantification of myocardial blood flow (MBF), providing improved diagnostic and prognostic performance and underscoring the need to reappraise myocardial perfusion imaging. This mini-review summarizes key physiological principles, contemporary acquisition and post-processing strategies, and the clinical relevance of myocardial perfusion imaging (MPI) across PET, Single Photon Emission Computed Tomography (SPECT), CMR, and CT, and discusses future perspectives in quantitative MPI.

## KEYWORDS

absolute myocardial blood flow, cardiac magnetic resonance (CMR), computed tomography (CT), myocardial perfusion imaging (MPI), pixel-wise quantification, positron emission tomography (PET), quantitative, single-photon emission computed tomography (SPECT)

## 1 Introduction: clinical indication for stress perfusion assessment

The SCOT-HEART trial (1) in 2018 highlighted the prognostic value of anatomical assessment with coronary computed tomography angiography (CCTA), shifting focus away from functional testing. Similarly, the COURAGE (2007) (2, 3) and ISCHEMIA (2020) (4) trials showed no reduction in coronary events with ischemia-guided revascularization compared with optimal medical therapy. Reflecting these findings, the 2021 American Heart Association chest pain guideline recommends CCTA as the first-line diagnostic test for intermediate-high risk patients with stable chest pain and no prior coronary artery disease (CAD) (5).

Nevertheless, myocardial perfusion assessment remains indispensable in known or suspected CAD, microvascular dysfunction, ischemia with normal coronary arteries (INOCA), coronary anomalies, and cardiomyopathies. The limitations of earlier perfusion-guided revascularization studies such as exercise stress testing, binary interpretations, and outdated protocols, underscore the need to reappraise myocardial perfusion imaging (MPI) (6). Modern positron emission tomography (PET),

cardiovascular magnetic resonance (CMR), and computed tomography (CT) techniques now enable absolute myocardial blood flow (MBF) quantification, offering improved diagnostic and prognostic performance (6, 7).

This mini-review summarizes key physiological principles, contemporary acquisition and post-processing strategies, and

the clinical relevance of PET, Single Photon Emission Computed Tomography (SPECT), CMR, and CT perfusion imaging, together with a summary table comparing key technical and workflow characteristics of quantitative MPI modalities (Table 1). We further discuss future perspectives in quantitative MPI.

TABLE 1 Comparisons of quantitative MPI modalities.

Characteristics	PET	SPECT	CMR	CT
Procedure time	20–45 min (19)	2.5–4 h (one-day protocols), up to two-day protocols (19)	30–60 min (7)	15–30 min (42)
Radiation Exposure	[ <sup>15</sup> O]H <sub>2</sub> O: ~0.4 mSv; [ <sup>13</sup> N]NH <sub>3</sub> : ~1 mSv; <sup>82</sup> Rb: ~0.7 mSv; [ <sup>18</sup> F]Flurpiridaz: ~4.6 mSv (6)	5–12 mSv (19, 21)	No radiation	Dynamic CT perfusion: 5.3 to 13.1mSv (42).
Spatial Resolution	4–6 mm, tracer-dependent (19) [ <sup>82</sup> Rb has relatively low spatial resolution. (12)]	10–15 mm [primarily determined by the collimator physics; CZT cameras have a twofold increase in image resolution compared with conventional SPECT cameras (21)]	Minimum spatial coverage is three slices in short-axis orientation, 2.5 × 2.5mm <sup>2</sup> in-plane, with a maximum slice thickness of 10 mm. (7)	Highest among all modalities, with sub-millimeter spatial resolution (42)
Temporal Resolution	PET detectors count events continuously; for dynamic PET, list-mode data are commonly binned into ~5-sec frames (62).	CZT SPECT detectors count events continuously; for dynamic SPECT, data are typically binned into 3–10 s frames (30).	High temporal resolution (<120 ms target readout temporal acquisition window), with an effective temporal resolution of one RR interval to ensure a consistent myocardial phase across the dynamic series (7).	The minimum gantry rotation time ranges from 250 to 400 ms, yielding an intrinsic temporal resolution of ~125–200 ms for single-source CT, while dual-source CT achieves ~65 ms temporal resolution. Dynamic acquisitions are typically repeated at 1–3 s intervals (42).
Renal Safety/Contrast Considerations	Generally safe in patients with reduced renal function	Generally safe in patients with reduced renal function	Macrocytic gadolinium agents may be used with caution in patients with severe renal impairment (38) (63).	Iodinated contrast is not recommended in patients with significantly reduced renal function. (64)
Availability	Mostly available in academic or high-volume centers. Requires a PET scanner (often hybrid PET/CT) and an on-site cyclotron for short-lived tracers.	Widely available. Most hospitals have SPECT cameras; CZT cameras are less common but increasingly adopted.	Moderate availability. Requires 1.5 T or 3 T MRI with cardiac capability and trained staff.	Moderate to high availability. Requires a multi-detector CT with perfusion capability (64+ slices or dual-source), which is common in many hospitals. Expertise for dynamic MPI may be limited.
Cost	Radiotracers are expensive, and scanner costs are the highest among all modalities.	Radiotracers are less expensive than PET tracers, and scanner costs are moderate.	Per-exam costs for gadolinium-based contrast agents are comparable to or lower than SPECT tracers; scanner costs are high.	Per-exam costs for iodinated contrast agents are the lowest among the modalities; scanner costs are high.
Key Features	Gold standard for quantitative myocardial perfusion and absolute blood flow measurement; emerging prognostic evidence; limited by high cost and specialized infrastructure.	Widely available and prognostically validated for relative perfusion; quantitative MBF measurement is possible with CZT cameras but less established and lower in accuracy compared with PET.	Excellent spatial and temporal fidelity without radiation; allows multiparametric assessment (perfusion, function, tissue characterization); sensitive to motion and operator-dependent.	Combines high-resolution perfusion imaging with coronary anatomy in a single study; rapid acquisition; limited by radiation and contrast nephrotoxicity.

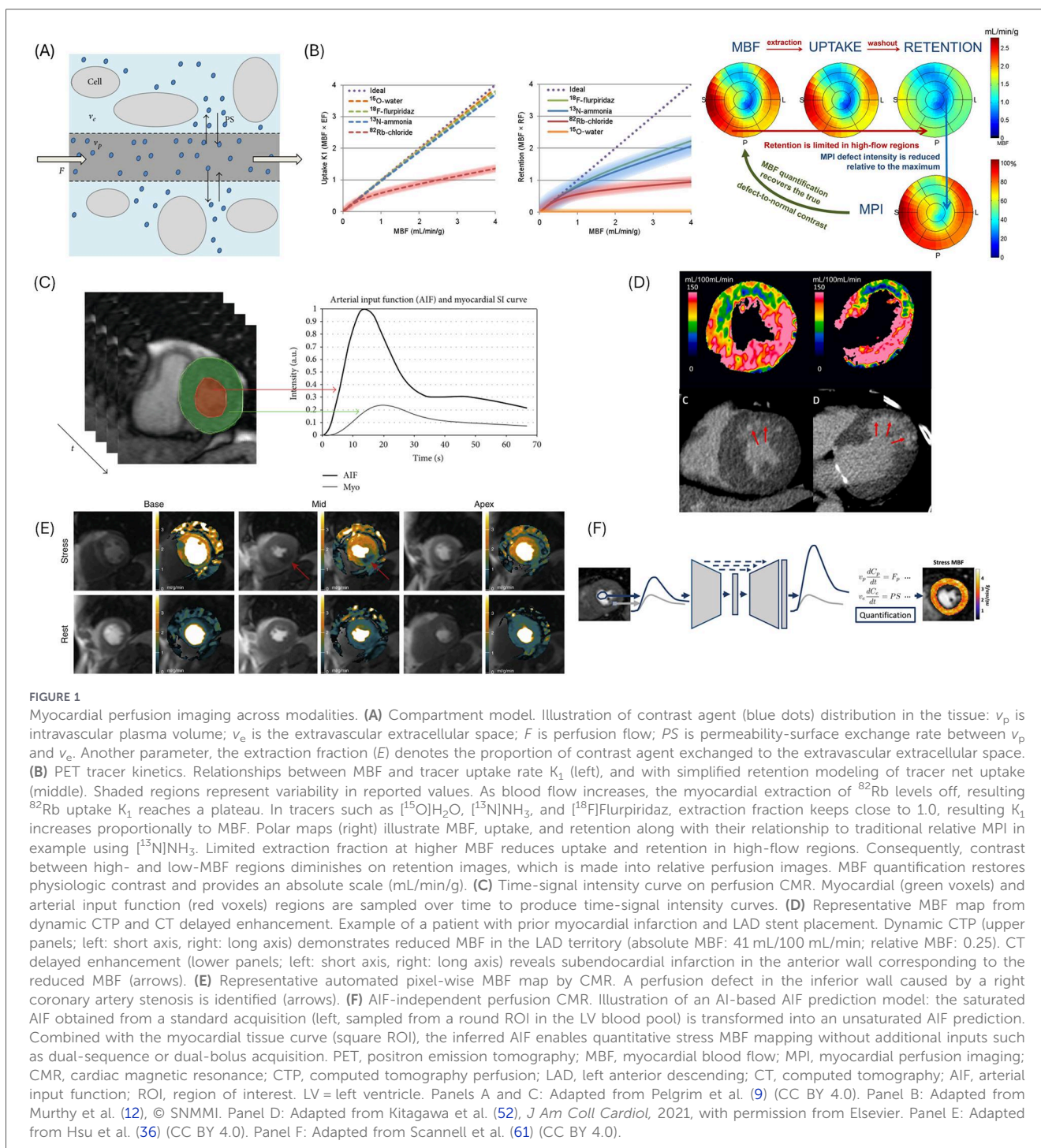
MPI, myocardial perfusion imaging; PET, positron emission tomography; SPECT, single-photon emission computed tomography; CMR, cardiovascular magnetic resonance; CT, computed tomography; MBF, myocardial blood flow; CZT, cadmium zinc telluride; MRI, magnetic resonance imaging.

## 2 Principles of myocardial perfusion modeling and the essential role of arterial input function (AIF)

Compartment modeling provides the foundation for quantitative MPI across modalities (8, 9). Understanding tracer or contrast kinetics and modeling strategies is crucial for quantitative analysis, inter-modality comparison, and physiological interpretation (10). Compartment models describe tracer exchange between intravascular and extravascular spaces, with or without a separate intracellular compartment. After delivery by blood flow, tracers cross the capillary wall into the

tissue by passive diffusion or active uptake, and may return to blood or be transiently retained in myocardium; some undergo intracellular trapping via binding or metabolism (Figure 1A) (11).

The two-compartment model is most physiologically relevant.  $K_1$  (mL/g/min) represents the unidirectional transfer from blood to myocardium, derived from dynamic time-activity curves (TACs), time-signal intensity curves, or time-attenuation curves (TACs) in the PET/SPECT, CMR, and CT, respectively.  $K_1$  reflects MBF (delivery term) and the extraction fraction (a dimensionless value between 0 and 1, reflecting fraction crossing the capillary membrane), and influenced by factors such as capillary permeability—surface area product, tracer or contrast properties



(molecular size, lipophilicity, protein binding, partition coefficient), tissue characteristics (fibrosis, edema), and physiological conditions (hematocrit, oxygen demand, vasodilator stress agents).  $K_2$  (mL/g/min) represents washout, determining the retention fraction. In a two-tissue model,  $K_3$  ( $\text{min}^{-1}$ ) represents intracellular trapping or metabolic conversion (Figure 1B) (12–14).

The arterial input function (AIF), typically obtained from the aorta or left ventricular (LV) cavity, characterizes the time-varying tracer or contrast concentration delivered to myocardium (Figure 1C). In PET, the injected dose and the first-pass extraction fraction are well characterized, often eliminating the need for explicit AIF measurement, though early studies used arterial blood sampling (11, 12). In CMR and CT, absolute MBF depends on deconvolution or compartment (tracer-kinetic) modeling. Deconvolution uses the shape of the AIF or tissue curves and not their absolute concentrations. During the time-signal intensity curve or TAC is deconvoluted with the AIF, the absolute concentration largely cancels out, isolating flow-dependent kinetics as the primary determinant of MBF (14). Compartment (tracer-kinetic) models need AIF as the input for modeling contrast exchange between compartments (9, 13). The absolute contrast concentration is directly used to fit the model and estimate  $K_1$  and  $K_2$ , providing physiologically meaningful parameters. Myocardial perfusion reserve (MPR), also referred to myocardial flow reserve (MFR), represents the ratio of stress to rest MBF. Importantly, MBF values are not interchangeable across modalities due to differences in extraction fraction, retention characteristics, and modeling assumptions (6, 7, 9, 12, 15). Modality-specific implementations are described in the following sections and summarized in Table 1.

### 3 Pharmacological stress agents

Modern MPI primarily uses pharmacological stress agents. Caffeine, a methylxanthine and competitive adenosine receptor antagonist, should be avoided at least 12 h before vasodilator administration (12). Common vasodilators include non-selective adenosine receptor agonists [adenosine, adenosine triphosphate (ATP), or dipyridamole] and the selective adenosine  $A_2A$  receptor agonist (regadenoson). Their plasma half-lives are <10 s (adenosine and ATP), 30–60 min (dipyridamole), and triphasic for regadenoson (2–4 min for initial distribution, ~30 min for intermediate, and ~2 h for terminal phase) (16). When stress precedes rest imaging, a sufficient time ( $\geq 10$  min) should be allowed for the patient return to baseline. Physiological responses (e.g., heart rate, blood pressure, or symptoms) should be monitored, and aminophylline (a non-selective adenosine receptor antagonist) is used in persistent or severe adverse effects such as prolonged atrioventricular block, bronchospasm, and severe hypotension (7, 17).

## 4 Stress perfusion by PET/SPECT

### 4.1 Image acquisition protocol and tracer characteristics

PET enables MBF measurement with superior spatial and contrast resolution, lower radiation, shorter procedural time, and higher diagnostic performance than SPECT (6, 18, 19).

Dynamic rest-stress imaging is standard (6, 12). CZT-SPECT MBF quantification remains challenging due to non-linear myocardial tracer uptake, but  $K_1$  estimation has been attempted (19). Detailed protocols are provided in the 2018 joint position paper of the Society of Nuclear Medicine and Molecular Imaging (SNMMI) and the American Society of Nuclear Cardiology (ASNC) (12), 2018 ASNC guidelines (20), and 2025 European Association of Cardiovascular Imaging (EACVI) consensus statement (21).

Common PET tracers include  $^{82}\text{Rb}$  ( $^{82}\text{Rb}$ ) and  $^{13}\text{N}$ -ammonia ( $[^{13}\text{N}]\text{NH}_3$ ), with  $^{15}\text{O}$ -water ( $[^{15}\text{O}]\text{H}_2\text{O}$ ) and  $^{18}\text{F}$ -Flurpiridaz ( $[^{18}\text{F}]\text{Flurpiridaz}$ ) mainly used in research (6, 11). Short half-life tracers ( $^{82}\text{Rb}$ : 76 s;  $[^{15}\text{O}]\text{H}_2\text{O}$ : 2.03 min) require on-site cyclotrons while enable fast stress and rest imaging with lower radiation dose. Longer half-life tracers ( $[^{13}\text{N}]\text{NH}_3$ : ~10 min;  $[^{18}\text{F}]\text{Flurpiridaz}$ : ~110 min) allow exercise stress. The representative SPECT tracers are  $^{201}\text{Tl}$  (half-life: 73 h) and  $^{99\text{m}}\text{Tc}$ -labeled compounds such as sestamibi or tetrofosmin (half-life: 6 h).  $^{201}\text{Tl}$  and  $^{82}\text{Rb}$  are potassium analogs transported into myocytes via  $\text{Na}^+/\text{K}^+$  pumps. Uptake of  $^{99\text{m}}\text{Tc}$ -sestamibi,  $^{99\text{m}}\text{Tc}$ -tetrofosmin, and  $[^{18}\text{F}]\text{Flurpiridaz}$  in the myocardium depends on intact mitochondria.  $[^{13}\text{N}]\text{NH}_3$  undergoes metabolic trapping, while  $[^{15}\text{O}]\text{H}_2\text{O}$  is metabolically inert and freely diffusible (11).

### 4.2 Assessment

Visual or semi-quantitative analysis, such as summed stress and rest scores (22) remain standard but may miss balanced or diffuse ischemia (12), whereas quantitative assessment provides a more complete evaluation of myocardial perfusion.

The radioactivity concentration (counts or kBq/mL) and the resulting shape of the TACs are determined by the tracer kinetics. Absolute MBF in PET is derived as  $K_1 = \text{MBF} \times \text{extraction fraction}$ . However, the non-linearity with different degrees is noted between  $K_1$  and MBF in high MBF ranges among tracers (Figure 1B). Freely diffusible tracers such as  $[^{15}\text{O}]\text{H}_2\text{O}$  can be modeled with a single compartment because they rapidly equilibrate between intra- and extravascular spaces, and their washout constant ( $K_2$ ) uniquely reflects MBF (6, 12). The cut-offs or reference values are heterogenous among literatures and by the tracers [Cut-offs: 1.7–2.5 mL/min/g for MBF; for MPR, threshold of 2.0 or 2.5 is often used (1.7–2.7 in range)] (6, 12). Reporting standards are outlined in the ASNC information statement (18).

### 4.3 Performance and prognostic value of stress PET and SPECT MPI

PET by qualitative and quantitative studies shows excellent diagnostic accuracy for detecting CAD, with pooled per-patient sensitivity and specificity of 84%–90% and 81%–88%, respectively (6). In a meta-analysis of 2048 patients across 37 studies (Takx et al., 2015), quantitative PET( $[^{15}\text{O}]\text{H}_2\text{O}$  MBF-PET), as well as MRI and CT including quantitative analysis, outperformed visual SPECT or echocardiography in ruling out FFR-defined significant CAD (patient-level sensitivity/specificity:

PET 84/87%, MRI 89/87%, CT 88/80%, SPECT 74/79%, echocardiography 69/84%) (23). Quantitative PET exceeds qualitative relative perfusion, regardless of tracer type (6). In [ $^{13}\text{N}$ ]NH $_3$  PET, absolute stress MBF outperformed relative uptake for detecting  $\geq 70\%$  stenosis by ICA (accuracy 84% vs. 72%,  $p < 0.01$ ) (24).

For prognostication in suspected or known CAD, impaired hyperemic MBF by [ $^{15}\text{O}$ ]H $_2\text{O}$  PET (<2.65 mL/min/g globally or <2.10 mL/min/g regionally) independently predicted death or myocardial infarction, after adjustment for clinical characteristics and MFR (global: HR = 2.55,  $p = 0.008$ ; regional: HR = 2.13,  $p = 0.04$ ) (Bom et al., 2020) (25). In another study, only MFR independently predicted MACE, outperforming absolute MBF (Benz et al., 2021) (26). Because MFR incorporates resting perfusion, it reflects broader physiological influences (e.g., hypertension, age) and offers a more comprehensive risk profile than MBF (6). Supporting this, a systematic review (Juárez-Orozco et al., 2018) of 6804 patients across 8 studies ( $^{82}\text{Rb}$ , [ $^{13}\text{N}$ ]NH $_3$ , [ $^{15}\text{O}$ ]H $_2\text{O}$ ) confirmed stronger prognostic value for MFR over stress MBF in predicting MACE and cardiac mortality (27). Longitudinal quantitative PET increasingly informs clinical decision-making (28, 29).

In head-to-head comparison with [ $^{15}\text{O}$ ]H $_2\text{O}$  PET, quantitative CZT-SPECT overestimated MBF, but MFR was comparable (30). In 303 CAD patients, including 100 INOCA (Li et al., 2023), SPECT-MFR <2.0 predicted higher MACE (log-rank  $P = 0.0019$ ), with each 1-unit increase reducing risk by  $\sim 66\%$  in INOCA and  $\sim 64\%$  overall (31). A meta-analysis (Baksa et al., 2025) confirmed diagnostic and prognostic value of CZT-SPECT MFR in suspected or known CAD, with pooled sensitivity 78.5% and specificity 89.3% vs. PET, and impaired SPECT-MFR independently predicting MACE (32).

## 5 Stress perfusion by CMR

### 5.1 Image acquisition protocol

The 2025 Society for Cardiovascular Magnetic Resonance (SCMR) Expert Consensus Statement recommends a stress-rest protocol with adenosine as the preferred vasodilator. Free-breathing sequences with motion correction are preferred, though breath-hold acquisitions remains acceptable (7).

AIF and high-resolution myocardial perfusion images can be obtained using dual bolus (DB) or dual sequence (DS). DB can be performed on any scanner but requires a diluted (10%;  $\sim 0.005\text{--}0.01$  mmol/kg) bolus followed by full-dose injection (0.05–0.1 mmol/kg). DS uses a single bolus with a low-resolution spoiled gradient echo with short-saturation preparation time (for AIF) followed by high-resolution perfusion imaging; it is easier to implement (33). In DS acquisition, high contrast concentration in the blood pool can cause signal deviation from linearity due to T1 and T2\* saturation effects, whereas in DB, the low-dose bolus for AIF keeps blood signal nonlinearity negligible in practice (7, 34, 35). Post-processing includes motion correction, signal non-linearity correction, baseline correction, coil sensitivity correction, and spatial filtering (7, 36). Detailed protocols are summarized in the 2025 SCMR Statement (7).

### 5.2 Assessment

Visual interpretation forms the basis of assessment, with limitations from inter-observer variability and dark-rim artifacts (37). Semi-quantitative “MPR” analysis uses the upslope or area under the myocardial time-signal intensity curve normalized to the LV blood pool (i.e., AIF); a stress/rest ratio >2 is generally considered normal (7). However, results depend on hemodynamics, imaging parameters, and contrast kinetics (13).

Quantitative perfusion CMR provides pixel-wise absolute MBF (mL/min/g) and MPR (i.e., MFR) with high spatial resolution (7). Although perfusion quantification is based on two compartment modeling (13), the high extraction fraction (effectively near 1 under clinical doses in CMR perfusion) and rapid gadolinium exchange allow practical use of single-compartment deconvolution approaches (10, 13, 33) (e.g., Fermi function/model-constrained deconvolution). Prior to deconvolution, DS requires AIF saturation correction and signal intensity-to-concentration conversion for both the AIF and myocardium, derived from two different sequences (7, 34, 35). In DB, this conversion can be bypassed, but scaling of the AIF by the dose ratio is required (13). Tracer-kinetic (compartmental) estimates the analogous to  $K_1$  by clearer physiological interpretation (8, 9). Conversion from signal intensity to concentration may be optional, as signal nonlinearities can be incorporated into the model. Perfusion defects are recommended to be reported as percentage of total myocardium (7).

### 5.3 Performance and prognostic value of stress CMR

Stress CMR demonstrates excellent diagnostic accuracy for hemodynamically significant CAD (38). In the CE-MARC study (2012) which visually scored the ischemic hypoperfusion (39), multiparametric CMR outperformed SPECT with higher sensitivity (86.5% vs. 66.5%) and similar specificity (83.4% vs. 82.6%). Fully automated pixel-wise MBF on DS imaging (Hsu et al., 2018) reported per-patient sensitivity and specificity of 82.9% and 80.0%, respectively, for detecting significant CAD by ICA. The stress and rest MBF from ischemic area was  $0.92 \pm 0.36$  and  $0.74 \pm 0.25$  mL/g/min, respectively, while  $3.67 \pm 0.79$  and  $1.22 \pm 0.33$  mL/g/min, respectively, in healthy volunteers (36).

For prognosis, MR-INFORM (2019) which followed 918 patients with stable angina for a median of 1 year, demonstrated less revascularization (35.7% vs. 45.0%,  $P = 0.005$ ) and non-inferiority for major outcomes at 1 year (3.6% vs. 3.7%) in visually semi-quantified CMR-guided strategy to FFR-guided management. Freedom from angina at 12 months was also similar (49.2% vs. 43.8%,  $p = 0.21$ ) (40). In a study using AI-derived MBF maps (Knott et al., 2020) on 1049 patients with suspected and known CAD, each 1 mL/g/min decrease in stress MBF predicted death (HR = 1.93,  $P = 0.028$ ) and MACE (HR = 2.14,  $P < 0.0001$ ). In a sub-group suspected for microvascular disease, MPR remained independently associated with death and MACE, with stress MBF remaining associated with MACE only (41).

## 6 Stress perfusion by cardiac CT

### 6.1 Image acquisition protocol

The Society of Cardiovascular Computed Tomography (SCCT) expert consensus recommends adding CT perfusion (CTP) for patients at high risk of obstructive CAD, including prior interventions or significant calcification, or stenoses of indeterminate functional significance (42). The choice of rest-first vs. stress-first depends on clinical context: patients with known CAD or extensive coronary calcium may undergo stress first, whereas coronary CTA is prioritized when anatomic information is lacking (42). Two primary approaches are static and dynamic CTP. Static CTP captures a single phase during contrast injection, enabling qualitative or semi-quantitative assessment; coronary CTA also serves as a resting static CTP. Reported radiation doses on 320-row scanners range from 2.5 to 9.3 mSv (42). Dynamic CTP acquires serial images during first-pass contrast to generate TACs proportional to MBF, with higher radiation exposure (5.3 to 13.1mSv) (42). Dual-energy CTP improves iodine visualization and mitigates beam-hardening and low contrast-to-noise ratio (CNR) issues (43), with reported doses of 4.2 to 16.5mSv (42). Dynamic CTP requires myocardial coverage (7–10 cm) during a 20–30 s breath-hold with high temporal resolution; shuttle mode is used in scanners with limited z-axis coverage, acquiring CT data at two alternate table positions by moving the table back and forth (42, 44). Detailed protocols are available in the 2020 SCCT expert consensus (42) and in publications (44, 45).

### 6.2 Assessment

In static CTP, absolute MBF is not assessable and perfusion defects are typically reported by the summed stress score (SSS) (42, 46). Dynamic CTP quantifies MBF typically using single-compartment indicator-dilution modeling and deconvolution (47), supported by the linear relationship between Hounsfield units (HU) and iodine concentration (48) (Figure 1D). Patlak tracer-kinetic approach estimates  $K_1$  via linear least-squares fitting without full multi-compartment modeling, simplifying the analytical procedures (14). Dynamic CTP also enables semi-quantitative TAC analysis normalized to AIF, with ischemic regions showing lower upslope and peak (49). CAD-RADS 2.0 CT reporting system incorporates ischemia detection as *modifier* “I”, with three severity categories of I+, I-, and I± (50).

### 6.3 Performance and prognostic value of stress CTP

Static stress CTP has been validated across multiple reference standards. In CORE320 (2014), static stress CTP plus coronary CTA was compared with stress SPECT in 381 patients with suspected or known CAD. Using  $\geq 50\%$  stenosis on ICA as reference, per-patient sensitivity and specificity were 88% and 55% for CTP vs. 62% and 67% for SPECT, with higher sensitivity in CTP for left main and multivessel disease (46). A 2019 meta-analysis of 5,330 patients from 54 studies comparing anatomical and functional CT for detecting FFR-defined significant CAD

demonstrated that CTP, from both dynamic and static studies, improved per-patient diagnostic accuracy over CTA (sensitivity and specificity: 83% and 79% for CTP; 94% and 48% for CTA). At the vessel level, dynamic CTP showed higher sensitivity (85% vs. 72%) but lower specificity (81% vs. 90%) than static CTP (51).

A multicenter dual-source dynamic stress CTP study (2021) utilized optimal cutoffs of 116 mL/100 mL/min (absolute MBF) and 0.71 (relative MBF) for detecting invasive FFR-defined significant stenoses. Dynamic CTP added incremental value over CTA, improving per-patient accuracy (from 64% to 74%,  $p < 0.001$ ) and specificity (from 36% to 75%,  $p < 0.001$ ), though with reduced sensitivity (from 93% to 72%,  $p < 0.001$ ) (52). A 2024 meta-analysis of 2190 patients from 23 studies reported pooled MBF of 0.92 vs. 1.39 mL/min/g in ischemic vs. non-ischemic regions ( $P < 0.001$ ). For detecting FFR-defined significant stenosis, patient-based pooled AUC was 0.92 with sensitivity 0.82 and specificity 0.86. CT-MBF also predicted adverse events (pooled HR = 4.98) (53).

Dynamic CTP also informs clinical decision making and prognostication. A 2020 study in patients with suspected CAD showed that a dynamic CTP-guided strategy significantly reduced angiography without revascularization compared with a CTA-only strategy (10.8% vs. 50.0%,  $p < 0.0001$ ) without increasing 1-year MACE (54). In a 2025 study of 226 patients followed for a median of 3.4 years, the relative MBF ratio (r-MBF), defined as the ratio of lowest to highest MBF regions, was the only independent predictor of MACE (HR = 0.82,  $p = 0.01$ ), whereas CT-FFR was not (55).

## 7 Discussion: future perspectives

Standardization of acquisition and analysis protocols is needed to mitigate variability in MBF within and across modalities, which are not yet interchangeable (6, 7, 9, 12, 15). Pixel-wise MBF mapping should become the dominant approach for future perfusion studies.

Advances in acquisition protocols, including DS acquisition in CMR, may improve accuracy and reproducibility. A notable topic not covered in earlier sections is non-contrast perfusion CMR based on native T1 mapping; it may expand access for patients with renal dysfunction and those requiring long-term follow-up (56, 57). CT perfusion is also progressing toward more quantitative perfusion assessment with lower contrast and radiation doses (42). Iodine mapping in spectral CTs such as dual-energy and photon-counting CT shows promise for future MBF quantification.

The wider adoption of AI-assisted workflows, including automated preprocessing, AIF detection and modeling (58), MBF map generation (36, 41), and prognostication (59), will further streamline analysis and reduce operator dependence (Figure 1E). Deep neural networks trained on large datasets can infer AIF from standard high-resolution perfusion images and may enable AIF-independent quantification in CMR and CT (Figure 1F) (60, 61).

## 8 Conclusion

Myocardial perfusion reflects both macrovascular and microvascular coronary flow, which deserves reappraisal with

modern PET, CMR, and CT techniques enabling absolute MBF with improved diagnostic and prognostic performance. Standardized acquisition and analysis protocols are warranted to mitigate variability in MBF measurements across modalities. AI-assisted workflows will further support broader clinical adoption of MPI.

## Author contributions

YK: Conceptualization, Writing – review & editing, Writing – original draft. OC: Writing – review & editing. BA-V: Supervision, Conceptualization, Writing – review & editing. JL: Supervision, Writing – review & editing.

## Funding

The author(s) declared that financial support was not received for this work and/or its publication.

## Conflict of interest

The author(s) declared that this work was conducted in the absence of any commercial or financial relationships that could be construed as a potential conflict of interest.

## References

1. SCOT-HEART Investigators, Newby DE, Adamson PD, Berry C, Boon NA, Dweck MR, Flather M, et al. Coronary CT angiography and 5-year risk of myocardial infarction. *N Engl J Med.* (2018) 379:924–33. doi: 10.1056/NEJMoa1805971
2. Boden WE, O'Rourke RA, Teo KK, Hartigan PM, Maron DJ, Kostuk WJ, et al. Optimal medical therapy with or without PCI for stable coronary disease. *N Engl J Med.* (2007) 356:1503–16. doi: 10.1056/NEJMoa070829
3. Shaw LJ, Berman DS, Maron DJ, Mancini GBJ, Hayes SW, Hartigan PM, et al. Optimal medical therapy with or without percutaneous coronary intervention to reduce ischemic burden: results from the clinical outcomes utilizing revascularization and aggressive drug evaluation (COURAGE) trial nuclear substudy. *Circulation.* (2008) 117:1283–91. doi: 10.1161/CIRCULATIONAHA.107.743963
4. Maron DJ, Hochman JS, Reynolds HR, Bangalore S, O'Brien SM, Boden WE, et al. Initial invasive or conservative strategy for stable coronary disease. *N Engl J Med.* (2020) 382:1395–407. doi: 10.1056/nejmoa1915922
5. Gulati M, Levy PD, Mukherjee D, Amsterdam E, Bhatt DL, Birtcher KK, et al. 2021 AHA/ACC/ASE/CHEST/SAEM/SCCT/SCMR guideline for the evaluation and diagnosis of chest pain: a report of the American College of Cardiology/American Heart Association joint committee on clinical practice guidelines. *Circulation.* (2021) 144:e368–454. doi: 10.1161/CIR.0000000000001029
6. Dahdal J, Jukema RA, Harms HJ, Cramer MJ, Raijmakers PG, Knaapen P, et al. PET Myocardial perfusion imaging: trends, challenges, and opportunities. *J Nucl Cardiol.* (2024) 40:102011. doi: 10.1016/j.nuclcard.2024.102011
7. Chiribiri A, Arai AE, DiBella E, Hsu L-Y, Ishida M, Jerosch-Herold M, et al. Society for cardiovascular magnetic resonance expert consensus statement on quantitative myocardial perfusion cardiovascular magnetic resonance imaging. *J Cardiovasc Magn Reson.* (2025) 27:101940. doi: 10.1016/j.jocmr.2025.101940
8. Tofts PS, Kermode AG. Measurement of the blood-brain barrier permeability and leakage space using dynamic MR imaging. 1. Fundamental concepts. *Magn Reson Med.* (1991) 17:357–67. doi: 10.1002/mrm.1910170208
9. Pelgrim GJ, Handayani A, Dijkstra H, Prakken NHJ, Slart RHJA, Oudkerk M, et al. Quantitative myocardial perfusion with dynamic contrast-enhanced imaging in MRI and CT: theoretical models and current implementation. *Biomed Res Int.* (2016) 2016:1734190. doi: 10.1155/2016/1734190
10. Jerosch-Herold M, Wilke N, Stillman AE, Wilson RF. Magnetic resonance quantification of the myocardial perfusion reserve with a Fermi function model for constrained deconvolution. *Med Phys.* (1998) 25:73–84. doi: 10.1118/1.598163

The authors YK, BA-V declared that they were an editorial board member of Frontiers at the time of submission. This had no impact on the peer review process and the final decision.

## Generative AI statement

The author(s) declared that generative AI was not used in the creation of this manuscript.

Any alternative text (alt text) provided alongside figures in this article has been generated by Frontiers with the support of artificial intelligence and reasonable efforts have been made to ensure accuracy, including review by the authors wherever possible. If you identify any issues, please contact us.

## Publisher's note

All claims expressed in this article are solely those of the authors and do not necessarily represent those of their affiliated organizations, or those of the publisher, the editors and the reviewers. Any product that may be evaluated in this article, or claim that may be made by its manufacturer, is not guaranteed or endorsed by the publisher.

11. Manabe O, Kikuchi T, Scholte AJHA, El Mahdoui M, Nishii R, Zhang MR, et al. Radiopharmaceutical tracers for cardiac imaging. *J Nucl Cardiol.* (2018) 25:1204–36. doi: 10.1007/s12350-017-1131-5
12. Murthy VL, Bateman TM, Beanlands RS, Berman DS, Borges-Neto S, Chareonthaitawee P, et al. Clinical quantification of myocardial blood flow using PET: joint position paper of the SNMMI cardiovascular council and the ASNC. *J Nucl Med.* (2018) 59:273–93. doi: 10.2967/jnumed.117.201368
13. Jerosch-Herold M. Quantification of myocardial perfusion by cardiovascular magnetic resonance. *J Cardiovasc Magn Reson.* (2010) 12:1–16. doi: 10.1186/1532-429X-12-57
14. Ichihara T, George RT, Silva C, Lima JAC, Lardo AC. Quantitative analysis of first-pass contrast-enhanced myocardial perfusion multidetector CT using a patlak plot method and extraction fraction correction during adenosine stress. *IEEE Trans Nucl Sci.* (2011) 58:133–8. doi: 10.1109/TNS.2010.2084104
15. Morton G, Chiribiri A, Ishida M, Hussain ST, Schuster A, Indermuehle A, et al. Quantification of absolute myocardial perfusion in patients with coronary artery disease: comparison between cardiovascular magnetic resonance and positron emission tomography. *J Am Coll Cardiol.* (2012) 60:1546–55. doi: 10.1016/j.jacc.2012.05.052
16. Cerqueira MD, Nguyen P, Staehr P, Underwood SR, Iskandrian AE, ADVANCE-MPI Trial Investigators. Effects of age, gender, obesity, and diabetes on the efficacy and safety of the selective A<sub>2A</sub> agonist regadenoson versus adenosine in myocardial perfusion imaging integrated ADVANCE-MPI trial results. *JACC: Cardiovasc Imaging.* (2008) 1:307–16. doi: 10.1016/j.jcmg.2008.02.003
17. Henzlova MJ, Duvall WL, Einstein AJ, Travin MI, Verberne HJ. ASNC Imaging guidelines for SPECT nuclear cardiology procedures: stress, protocols, and tracers. *J Nucl Cardiol.* (2016) 23:606–39. doi: 10.1007/s12350-015-0387-x
18. Chareonthaitawee P, Bateman TM, Beanlands RS, Berman DS, Calnon DA, Di Carli MF, et al. Atlas for reporting PET myocardial perfusion imaging and myocardial blood flow in clinical practice: an information statement from the American society of nuclear cardiology. *J Nucl Cardiol.* (2023) 30:2850–906. doi: 10.1007/s12350-023-03378-1
19. Alwan M, El Ghazawi A, El Yaman A, Al Rifai M, Al-Mallah MH. SPECT Myocardial perfusion imaging in the era of PET and multimodality imaging: challenges and opportunities. *Prog Cardiovasc Dis.* (2025) 93:3–9. doi: 10.1016/j.pcad.2025.09.002

20. Dorbala S, Ananthasubramaniam K, Armstrong IS, Chareonthaitawee P, DePuey EG, Einstein AJ, et al. Single photon emission computed tomography (SPECT) myocardial perfusion imaging guidelines: instrumentation, acquisition, processing, and interpretation. *J Nucl Cardiol.* (2018) 25:1784–846. doi: 10.1007/s12350-018-1283-y
21. Abadie B, Liga R, Buechel R, Giannopoulos AA, Pizzi MN, Roque A, et al. Patient centric performance and interpretation of SPECT and SPECT/CT myocardial perfusion imaging: a clinical consensus statement of the European association of cardiovascular imaging of the ESC. *Eur Hear J Imaging Methods Pract.* (2025) 3: qyaf043. doi: 10.1093/ehjimp/qyaf043
22. Greenwood JP, Maredia N, Radjenovic A, Brown JM, Nixon J, Farrin AJ, et al. Clinical evaluation of magnetic resonance imaging in coronary heart disease: the CE-MARC study. *Trials.* (2009) 10:62. doi: 10.1186/1745-6215-10-62
23. Takx RAP, Blomberg BA, El Aidi H, Habets J, de Jong PA, Nagel E, et al. Diagnostic accuracy of stress myocardial perfusion imaging compared to invasive coronary angiography with fractional flow reserve meta-analysis. *Circ Cardiovasc Imaging.* (2015) 8:e002666. doi: 10.1161/CIRCIMAGING.114.002666
24. Hajjiri MM, Leavitt MB, Zheng H, Spooner AE, Fischman AJ, Gewirtz H. Comparison of positron emission tomography measurement of adenosine-stimulated absolute myocardial blood flow versus relative myocardial tracer content for physiological assessment of coronary artery stenosis severity and location. *JACC Cardiovasc Imaging.* (2009) 2:751–8. doi: 10.1016/j.jcmg.2009.04.004
25. Bom MJ, Van Diemen PA, Driessen RS, Everaars H, Schumacher SP, Wijmenga JT, et al. Prognostic value of [15O]H<sub>2</sub>O positron emission tomography-derived global and regional myocardial perfusion. *Eur Heart J Cardiovasc Imaging.* (2020) 21:777–86. doi: 10.1093/ehjci/jez258
26. Benz DC, Kaufmann PA, von Felten E, Benetos G, Rampidi G, Messerli M, et al. Prognostic value of quantitative metrics from positron emission tomography in ischemic heart failure. *JACC Cardiovasc Imaging.* (2021) 14:454–64. doi: 10.1016/j.jcmg.2020.05.033
27. Juárez-Orozco LE, Tio RA, Alexanderson E, Dweck M, Vliegenthart R, El Moumni M, et al. Quantitative myocardial perfusion evaluation with positron emission tomography and the risk of cardiovascular events in patients with coronary artery disease: a systematic review of prognostic studies. *Eur Heart J Cardiovasc Imaging.* (2018) 19:1179–87. doi: 10.1093/ehjci/jex331
28. Assante R, Zampella E, D'Antonio A, Mannarino T, Gaudieri V, Nappi C, et al. Impact on cardiovascular outcome of coronary revascularization-induced changes in ischemic perfusion defect and myocardial flow reserve. *Eur J Nucl Med Mol Imaging.* (2024) 51:1612–21. doi: 10.1007/s00259-023-06588-4
29. Wiefels C, Almuehleh A, Yao J, deKemp RA, Chong AY, Mielniczuk LM, et al. Prognostic utility of longitudinal quantification of PET myocardial blood flow early post heart transplantation. *J Nucl Cardiol.* (2022) 29:712–23. doi: 10.1007/s12350-020-02342-7
30. Agostini D, Roule V, Nganoa C, Roth N, Baavour R, Parienti JJ, et al. First validation of myocardial flow reserve assessed by dynamic 99mTc-sestamibi CZT-SPECT camera: head to head comparison with 15O-water PET and fractional flow reserve in patients with suspected coronary artery disease. The WATERDAY Study. *Eur J Nucl Med Mol Imaging.* (2018) 45:1079–90. doi: 10.1007/s00259-018-3958-7
31. Li L, Pang Z, Wang J, Chen Y, Chu H, He Z, et al. Prognostic value of myocardial flow reserve measured with CZT cardiac-dedicated SPECT low-dose dynamic myocardial perfusion imaging in patients with INOCA. *J Nucl Cardiol.* (2023) 30:2578–92. doi: 10.1007/s12350-023-03332-1
32. Baksa B, Reddy SS, Bundula S, Nagy K, Beke S, Száraz L, et al. Diagnostic and prognostic value of myocardial flow reserve quantification with single photon emission computed tomography—a systematic review and meta-analysis. *EJNMMI Res.* (2025) 15:139. doi: 10.1186/s13550-025-01335-2
33. Kellman P, Hansen MS, NIELLES-Vallespin S, Nickander J, Themudo R, Ugander M, et al. Myocardial perfusion cardiovascular magnetic resonance: optimized dual sequence and reconstruction for quantification. *J Cardiovasc Magn Reson.* (2017) 19:1–14. doi: 10.1186/s12968-017-0355-5
34. Utz W, Niendorf T, Wassmuth R, Messroghli D, Dietz R, Schulz-Menger J. Contrast-dose relation in first-pass myocardial MR perfusion imaging. *J Magn Reson Imaging.* (2007) 25:1131–5. doi: 10.1002/jmri.20910
35. Hsu LY, Kellman P, Arai AE. Nonlinear myocardial signal intensity correction improves quantification of contrast-enhanced first-pass MR perfusion in humans. *J Magn Reson Imaging.* (2008) 27:793–801. doi: 10.1002/jmri.21286
36. Hsu LY, Jacobs M, Benovoy M, Ta AD, Conn HM, Winkler S, et al. Diagnostic performance of fully automated pixel-wise quantitative myocardial perfusion imaging by cardiovascular magnetic resonance. *JACC Cardiovasc Imaging.* (2018) 11:697–707. doi: 10.1016/j.jcmg.2018.01.005
37. Schulz-Menger J, Bluemke DA, Bremerich J, Flamm SD, Fogel MA, Friedrich MG, et al. Standardized image interpretation and post-processing in cardiovascular magnetic resonance—2020 update. *J Cardiovasc Magn Reson.* (2020) 22:1–22. doi: 10.1186/s12968-020-00610-6
38. Kwong RY, Heydari B, Bernhard B. A practical review of stress perfusion cardiac magnetic resonance imaging for the management of coronary artery disease. *Curr Opin Cardiol.* (2025) 40:448–58. doi: 10.1097/HCO.0000000000001259
39. Greenwood JJP, Maredia N, Younger JFJ, Brown JM, Nixon J, Everett CC, et al. Cardiovascular magnetic resonance and single-photon emission computed tomography for diagnosis of coronary heart disease (CE-MARC): a prospective trial. *Lancet.* (2012) 379:453–60. doi: 10.1016/S0140-6736(11)61335-4
40. Nagel E, Greenwood JP, McCann GP, Bettencourt N, Shah AM, Hussain ST, et al. Magnetic resonance perfusion or fractional flow reserve in coronary disease. *N Engl J Med.* (2019) 380:2418–28. doi: 10.1056/nejmoa1716734
41. Knott KD, Seraphim A, Augusto JB, Xue H, Chacko L, Aung N, et al. The prognostic significance of quantitative myocardial perfusion: an artificial intelligence-based approach using perfusion mapping. *Circulation.* (2020) 141:1282–91. doi: 10.1161/CIRCULATIONAHA.119.044666
42. Patel AR, Bamberg F, Branch K, Carrascosa P, Chen M, Cury RC, et al. Society of cardiovascular computed tomography expert consensus document on myocardial computed tomography perfusion imaging. *J Cardiovasc Comput Tomogr.* (2020) 14:87–100. doi: 10.1016/j.jcct.2019.10.003
43. Scherer K, Hammel J, Sellaer T, Mechlem K, Renger B, Bähr A, et al. Dynamic quantitative iodine myocardial perfusion imaging with dual-layer CT using a porcine model. *Sci Rep.* (2019) 9:16046. doi: 10.1038/s41598-019-52458-1
44. Møller MB, Schuijff JD, Oyama-Manabe N, Linde JJ, Kühl JT, Lima JAC, et al. Technical considerations for dynamic myocardial computed tomography perfusion as part of a comprehensive evaluation of coronary artery disease using computed tomography. *J Thorac Imaging.* (2023) 38:54–68. doi: 10.1097/RTI.0000000000000673
45. Chehab O, De Vasconcellos HD, Lima J. Myocardial perfusion and viability CT imaging. In: Zadeh AA, John Hoe J, editors. *Practical Guide to Cardiac CT.* Singapore: Springer Nature Singapore (2024). p. 215–26.
46. George RT, Mehra VC, Chen MY, Kitagawa K, Arbab-Zadeh A, Miller JM, et al. Myocardial CT perfusion imaging and SPECT for the diagnosis of coronary artery disease: a head-to-head comparison from the CORE320 multicenter diagnostic performance study. *Radiology.* (2014) 272:407–16. doi: 10.1148/radiol.14140806
47. Nous FMA, Geisler T, Kruk MBP, Alkadhhi H, Kitagawa K, Vliegenthart R, et al. Dynamic myocardial perfusion CT for the detection of hemodynamically significant coronary artery disease. *JACC Cardiovasc Imaging.* (2022) 15:75–87. doi: 10.1016/j.jcmg.2021.07.021
48. Bae KT. Intravenous contrast medium administration and scan timing at CT: considerations and approaches. *Radiology.* (2010) 256:32–61. doi: 10.1148/radiol.10090908
49. George RT, Jerosch-Herold M, Silva C, Kitagawa K, Bluemke DA, Lima JAC, et al. Quantification of myocardial perfusion using dynamic 64-detector computed tomography. *Invest Radiol.* (2007) 42:815–22. doi: 10.1097/RLI.0b013e318124a884
50. Cury RC, Leipsic J, Abbara S, Achenbach S, Berman D, Bittencourt M, et al. CAD-RADS™ 2.0 - 2022 coronary artery disease-reporting and data system: an expert consensus document of the society of cardiovascular computed tomography (SCCT), the American College of Cardiology (ACC), the American college of radiology (ACR), and the No. *J Cardiovasc Comput Tomogr.* (2022) 16:536–57. doi: 10.1016/j.jcct.2022.07.002
51. Celeng C, Leiner T, Maurovich-Horvat P, Merkely B, de Jong P, Dankbaar JW, et al. Anatomical and functional computed tomography for diagnosing hemodynamically significant coronary artery disease: a meta-analysis. *JACC Cardiovasc Imaging.* (2019) 12:1316–25. doi: 10.1016/j.jcmg.2018.07.022
52. Kitagawa K, Nakamura S, Ota H, Ogawa R, Shizuka T, Kubo T, et al. Diagnostic performance of dynamic myocardial perfusion imaging using dual-source computed tomography. *J Am Coll Cardiol.* (2021) 78:1937–49. doi: 10.1016/j.jacc.2021.08.067
53. Kawaguchi Y, Kato S, Horita N, Utsunomiya D. Value of dynamic computed tomography myocardial perfusion in CAD: a systematic review and meta-analysis. *Eur Hear J - Cardiovasc Imaging.* (2024) 25:1675–85. doi: 10.1093/ehjci/jeae118
54. Yu M, Shen C, Dai X, Lu Z, Wang Y, Lu B, et al. Clinical outcomes of dynamic computed tomography myocardial perfusion imaging combined with coronary computed tomography angiography versus coronary computed tomography angiography-guided strategy. *Circ Cardiovasc Imaging.* (2020) 13:E009775. doi: 10.1161/CIRCIMAGING.119.009775
55. Yi Y, Li D, Xu C, Zou L, Yu XB, Wang M, et al. Prognostic significance of stress dynamic myocardial CT perfusion: comparison with CT-FFR and CT angiography stenosis—the multicenter VALIDITY trial. *Eur Radiol.* (2025) 35:2899–909. doi: 10.1007/s00330-024-11187-4
56. Nakamori S, Fahmy A, Jang J, El-Rewaady H, Neisius U, Berg S, et al. Changes in myocardial native T1 and T2 after exercise stress: a noncontrast CMR pilot study. *JACC Cardiovasc Imaging.* (2020) 13:667–80. doi: 10.1016/j.jcmg.2019.05.019
57. Nickander J, Steffen Johansson R, Lodin K, Wahrby A, Loewenstein D, Bruchfeld J, et al. Stress native T1 and native T2 mapping compared to myocardial perfusion reserve in long-term follow-up of severe COVID-19. *Sci Rep.* (2023) 13:4159. doi: 10.1038/s41598-023-30989-y
58. van Herten RLM, Chiribiri A, Breeuwer M, Veta M, Scannell CM. Physics-informed neural networks for myocardial perfusion MRI quantification. *Med Image Anal.* (2022) 78:102399. doi: 10.1016/j.media.2022.102399
59. Hu X, Zhang H, Caobelli F, Huang Y, Li Y, Zhang J, et al. The role of deep learning in myocardial perfusion imaging for diagnosis and prognosis: a systematic review. *iScience.* (2024) 27:111374. doi: 10.1016/j.isci.2024.111374

60. de la Rosa E, Sima DM, Menze B, Kirschke JS, Robben D. AIFNet: automatic vascular function estimation for perfusion analysis using deep learning. *Med Image Anal.* (2021) 74:102211. doi: 10.1016/j.media.2021.102211
61. Scannell CM, Alskaf E, Sharrack N, Razavi R, Ourselin S, Young AA, et al. AI-AIF: artificial intelligence-based arterial input function for quantitative stress perfusion cardiac magnetic resonance. *Eur Hear J - Digit Heal.* (2023) 4:12–21. doi: 10.1093/ehjdh/ztac074
62. O' Doherty J, Chalampalakos Z, Schleyer P, Nazir MS, Chiribiri A, Marsden PK. The effect of high count rates on cardiac perfusion quantification in a simultaneous PET-MR system using a cardiac perfusion phantom. *EJNMMI Phys.* (2017) 4:31. doi: 10.1186/s40658-017-0199-y
63. Weinreb JC, Rodby RA, Wang YJ, Fine CL, McDonald D, Perazella RJ, et al. Use of intravenous gadolinium-based contrast media in patients with kidney disease: consensus statements from the American college of radiology and the national kidney foundation. *Radiology.* (2021) 298:28–35. doi: 10.1148/RADIOL.2020202903
64. Contrast Media Safety Committee. ESUR Guidelines on contrast agents v10.0. *Eur Soc Urogenit Radiol.* (2018):0–45. Available online at: [http://www.esur.org/fileadmin/content/2019/ESUR\\_Guidelines\\_10.0\\_Final\\_Version.pdf](http://www.esur.org/fileadmin/content/2019/ESUR_Guidelines_10.0_Final_Version.pdf) (Accessed February 09, 2026).